PAPER

Synthesis and optical nonlinear properties performance of azonaphthol dye

Physica Scripta

PAPER

Synthesis and optical nonlinear properties performance of azonaphthol dye

RECEIVED
7 November 2020

REVISED
26 November 2020

ACCEPTED FOR PUBLICATION
8 December 2020

PUBLISHED
16 December 2020

Ahmed Majeed Jassem[1], **Qusay M A Hassan**[2], **C A Emshary**[2], **H A Sultan**[2], **Faeza Abdulkareem Almashal**[1] **and Wisam Abdulhassan Radhi**[3]

[1] Department of Chemistry, College of Education for Pure Sciences, Basrah University, Basrah, Iraq
[2] Department of Physics, College of Education for Pure Sciences, Basrah University, Basrah, Iraq
[3] Department of Chemistry, Polymer Research Center, Basrah University, Basrah, Iraq

E-mail: qusayali64@yahoo.co.in

Keywords: azonaphthol dye, spatial self-phase modulation, nonlinear index of refraction, diffraction ring pattern, optical limiting

Abstract

Azonapthol dye viz., (E)-4-(phenyldiazenyl)naphthalen-1-ol ($C_{16}H_{11}N_3O_3$) is synthesized via diazotization of *p*-nitro aniline and subsequent coupling with α-naphthol. 1H NMR spectrum is used to identify the position of protons in obtained compound. FTIR spectrum is used to assign the absorption bands of vibration bonds at the expected regions. Mass spectrum proved a good agreement with structure of the prepared azonaphthol dye. The third order optical nonlinear properties of the azonaphthol dye **4** dissolved in acetone viz., the nonlinear index of refraction and the nonlinear absorption are obtained using 473 nm laser beam via diffraction ring patterns at 42 mW and Z-scan at 5 mW techniques separately. High nonlinear refractive index, 10^{-6} cm^2 W^{-1}, is obtained via diffraction ring pattern. Optical limiting property of azonapthol dye **4** solution is tested and a limiting threshold value of 17 mW is obtained, and prove that the sample can be used as an optical limiter. The Fraunhofer approximations of the Fresnel-Kirchhoff theory have led to the diffraction ring patterns simulation where very good agreement have been obtained.

1. Introduction

During the last thirty years a continuing interest in development and exploring of new materials with nonlinear optical properties owe to the possible applications in optical modulation, all optical switching, telecommunication, optical memory devices, data storage, protection of optical sensors and human eyes, etc [1–15]. Organic materials being the prime materials that have been studied extensively for these purposes [16–20]. They show excellent optical nonlinear properties and large nonlinearities, easy molecular design, fast response time, and good ability to process to build optical devices [21].

When a laser beam traverses a nonlinear medium number of spatial effects occurs viz., spatial ring formation, beam break-up, self-focusing and self-defocusing and thermal lens formation. The spatial ring formation was discovered in 1967 by Callen *et al* [22], then it was demonstrated that such diffraction ring patterns can be used in the determination of the change of the medium index of refraction and the nonlinear index of refraction. During 1990 Shake bahae *et al* pioneered the Z-scan technique [23] which can be used in the calculation of the coefficient of nonlinear absorption, the nonlinear index of refraction, the optical nonlinear susceptibility of the nonlinear medium and the assignment of the sign of the nonlinear index of refraction and coefficient of nonlinear absorption. Based on the diffraction ring patterns, the Z-scan and the thermal lens so many materials have been proved to behave nonlinearly in response to the propagation of low power, sub-Watt, with Gaussian intensity distribution laser beams [24–28].

Azo compounds or the compounds that bear an azo group (-N = N- group) gain importance in organic and industrial chemistry. The azo materials optical nonlinear response might be attributed to either electronic process or to nonelectronic process or to both. The first one results from the bound electrons nonlinear response. The second one is due to nonradiation interaction for instance the change in density, cis-trans

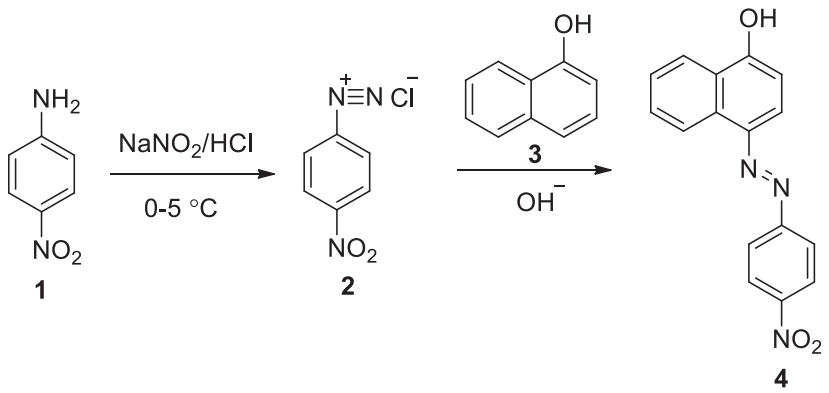

Figure 1. Synthesis of azonaphthol dye **4.**

isomerization, and temperature. Azo compounds have received much attention in the search for bioactive agents [29–31] as they are useful compounds for synthesis of pharmacological agents such as HIV inhibitor [32] and drug delivery [33]. Azo compounds offer diverse applications in high and modern technology fields including thermo chromic properties, optical computers to measure radiation intensity, imaging systems, molecular memory storage, photo stabilizers, reversible optical memories, photo detectors in biological system, solar collectors, and solar filters [34–36]. In addition, they are also used in liquid crystals [37], smart molecules [38], molecular motors [39], corrosion inhibition [40–42] and sensitizers [43]. The nonlinear optical properties [44–49], the optical switching, and optical phase conjugation [50, 51] of azo compounds have been studies during the last twenty years. Azo compounds studied for different reasons too [52–56].

Presently, chemists and physicists are looking for new materials with optical nonlinear applications in photonics, optoelectronics and nanophotonics by using either ultra-short pulsed lasers [57] or continuous wave diode-pumped lasers [58]. Organic dye compounds are able to absorb part of laser beam light in the visible region (400–700 nm). The absorption spectra of azo compounds consist of number of absorption bands at various intensities that usually overlap due to the transfer of electrons from different energy levels [59]. They display resonance of electrons (conjugated systems) which represent as a stabilizing force and to modify the hyperpolarizability in these compounds with highly potential nonlinear optical properties. As far as we know the azonaphthol dye **4** optical and nonlinear optical properties have received little attention by the researchers [60–62]. In the present work the optical nonlinear properties viz., the nonlinear index of refraction and the coefficient of nonlinear absorption of a prepared azonaphthol dye **4** (figure 1) are studied using a continuous wave (CW) laser beam of wavelength 473 nm by the two techniques viz. (i) diffraction ring patterns and (ii) Z-scan.

2. Experimental section

2.1. Diffraction ring pattern

The diffraction ring patterns usually obtained using the set-up mentioned in our previous work [15]. It consist of CW, single transvers fundamental TEM_{00}, mode laser beam of wavelength 473 nm emitted by a solid state, diode pumped laser device type SDL-473–100 T with 66 mW maximum output power, a short focal length glass positive lens ($f = 50$ mm) for the sake of focusing the laser beam onto the sample in 1 mm thickness glass cell and a semitransparent screen (30×30 cm), which was 80 cm away from sample cell exit plane i.e., in the far field to cast the diffraction ring patterns.

2.2. Z-scan

The Z-scan was conducted via the use of the same set-up described subsection 2.1 where the sample usually fixed on a translation stage to scan the sample across the same positive glass lens along the z-direction passing through its focus ($z = 0$) between ($-z$) to ($+z$), the screen was replaced with an optical detector covered by a circular aperture of 2 mm diameter. Closed aperture, CA, Z-scan was conducted via by this set-up while the open aperture, OA, Z-scan was carried out using the same set up and the aperture replaced by a power meter and a positive glass lens.

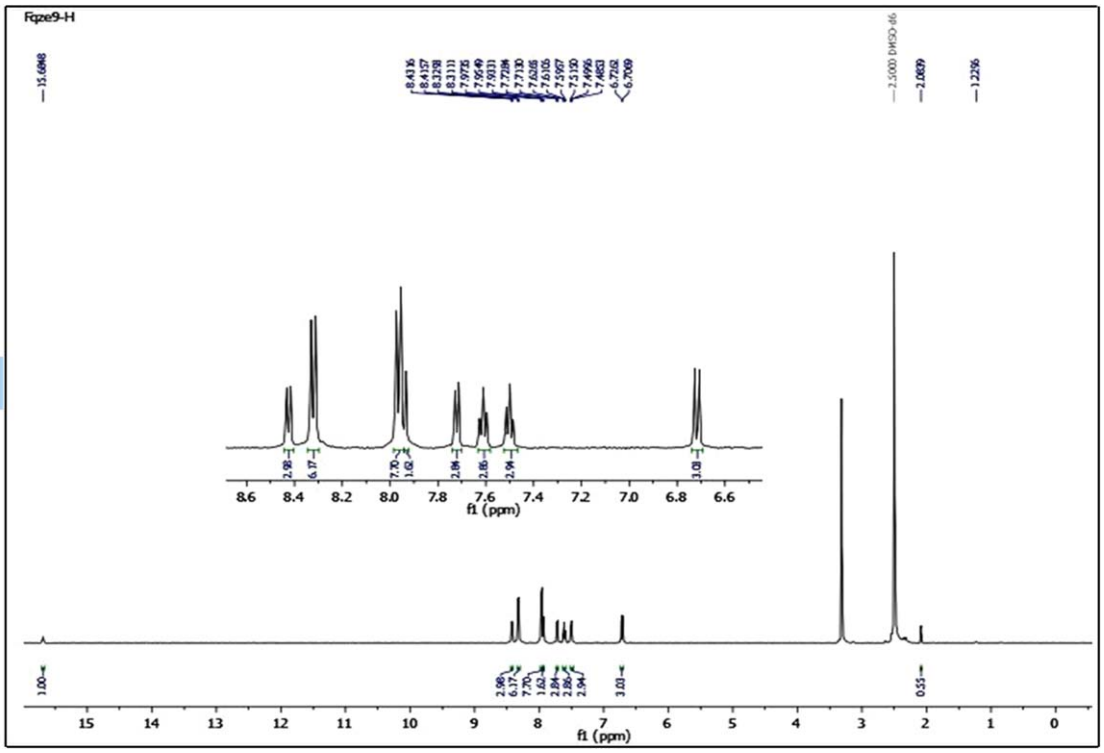

Figure 2. ^{1}H NMR spectrum of azonaphthol dye **4**.

2.3. Optical limiting

In this part the sample usually positioned behind the lens focal point i.e. in the valley position of the CA Z-scan. The input power varied and recording the power of the laser beam leaving the sample cell.

2.4. Materials and methods

Without further purification all the chemicals and solvents, were used. From Sigma-Aldrich all the chemicals and solvents were obtained. Progress of the reactions prepress was monitored by Thin-layer chromatography TLC using silica gel G/UV 254 plates. The 1H-NMR spectrum was run on a Bruker inovo AV-400 spectrometer at room temperature in detuerated dimethyl sulfoxide (DMSO-d_6) as solvent with a signal peak of ^{1}H spectrum at δ 2.50 ppm (TMS as internal reference). The completed proton of decoupling values (J) are introduced in Hz. FTIR spectrum was recorded on Shimadzu FTIR-84005 infrared spectrophotometer using KBr disk and the absorbance was taken in the range 3600–600 cm^{-1}. Melting points were obtained using a Gallenkamp melting point apparatus in capillary tubes. Accurate mass was recorded on a Micro Mass LCT operating in Electrospray impact mode (EI). The Ultraviolet-visible (UV-vis) spectrum was performed by using UV-160v, Shimadzu spectrophotometer at the regions (350–900 nm).

2.4.1. Synthesis of diazonium salt 2

p-Nitro aniline **1** (10 mmol) was stirred in con. hydrochloric acid (15 ml) until a clear solution appeared. The resulting mixture was cooled to 0–5 °C by using an ice bath. A cold solution of sodium nitrite $NaNO_2$ (50 ml) was added drop-wise to the acidified amine solution, maintaining the temperature of the mixture between 0–5 °C. The resulting solution was stirred for further 45 min below 5 °C to afford a diazonium salt **2** which was immediately used in the next step (coupling reaction).

2.4.2. Synthesis of azonaphthol dye 4 (coupling reaction)

A mixture of α-naphthol **3** (coupling partner) (10 mmol) in NaOH (3 M, 40 ml) was cooled to 0–5 °C in an ice bath. The obtained solution was then added to the cold benzenediazonium salt **2** and the resulting mixture was stirred slowly below 5 °C for 60 min. The precipitated red crystals were collected by filtration, thoroughly washed with an ice water, dried and recrystallized from methanol gave azonaphthol dye **4** ($C_{16}H_{11}N_3O_3$), m.p. 123–124 °C.

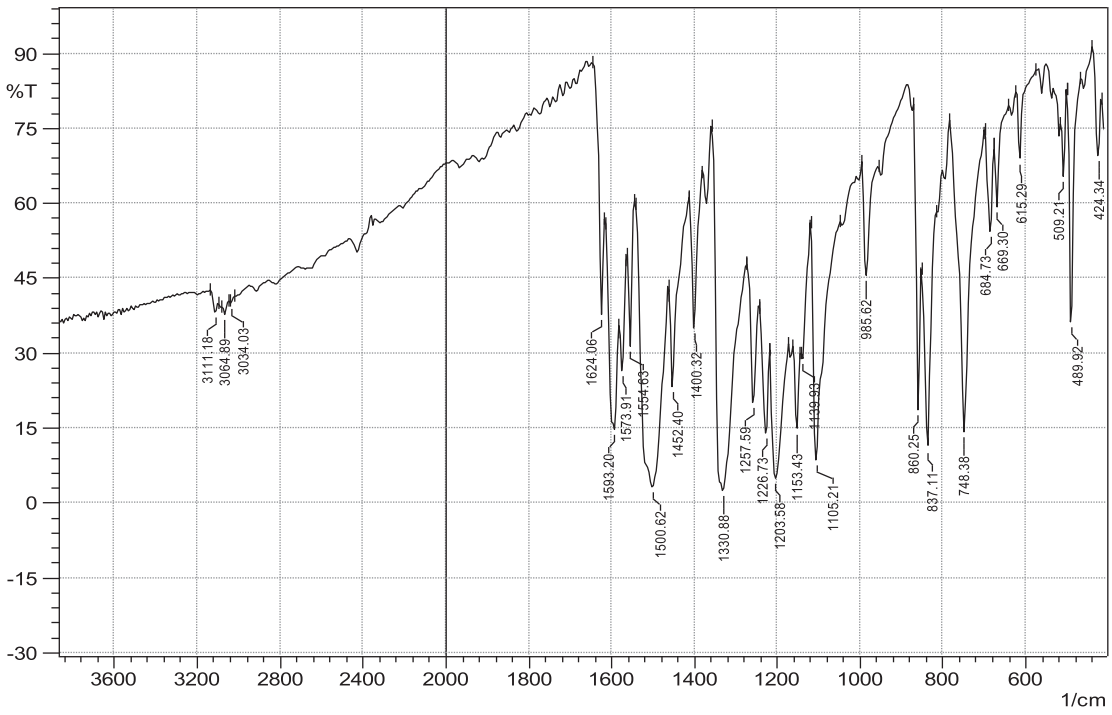

Figure 3. FTIR spectrum of azonaphthol dye **4**.

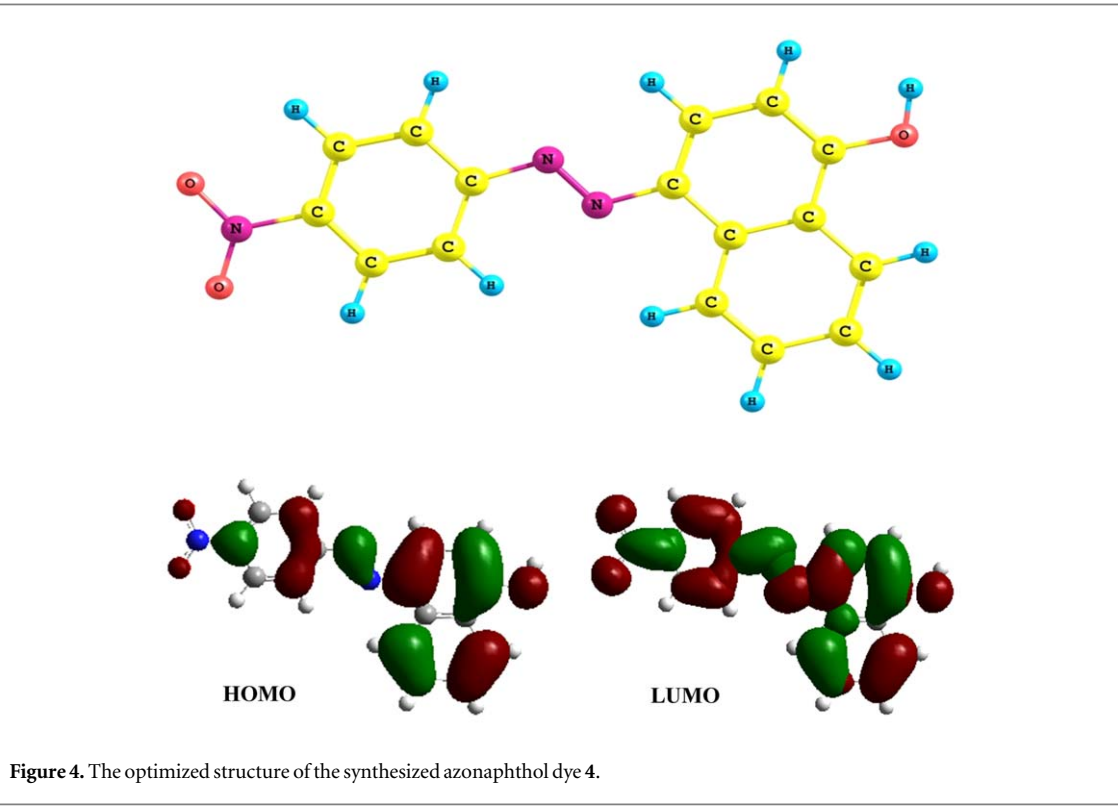

Figure 4. The optimized structure of the synthesized azonaphthol dye **4**.

2.5. ^{1}H NMR spectrum

The ^{1}H NMR spectrum of azonaphthol dye **4** was measured in DMSO- d_6. The ^{1}H data of the synthesized azonaphthol dye **4** is completely consistent with the expected structure. Phenolic group (OH) in azonaphthol dye **4** appeared at 15.68 ppm as a broad singlet at the lowest field (1H, br, s).

The ^{1}H NMR spectrum also shows multiplet signals at 6.72–8.43 ppm for aromatic protons at the expected region. The ^{1}H NMR spectrum of azonaphthol dye **4** is displayed in figure 2.

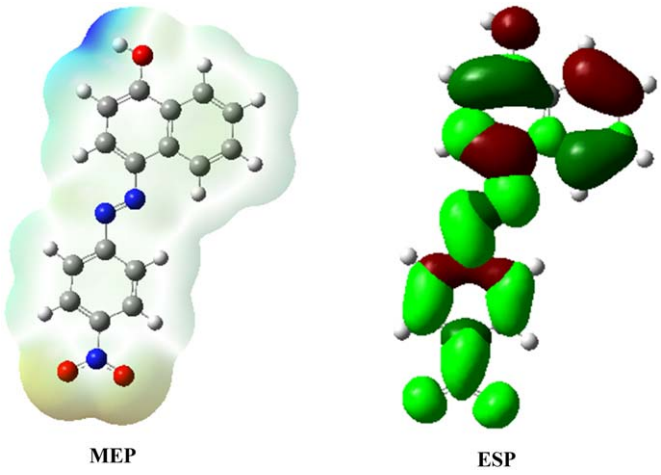

Figure 5. MEP and ESP maps of the synthesized azonaphthol dye **4**.

Table 1. Important physico-chemical properties of the synthesized azonaphthol dye **4**.

Molecule	E_{HOMO} (eV)	E_{LUMO} (eV)	ΔE.Gap (eV)	Dipole moment(Debye)	Total energy (eV)
Azonaphthol dye 4	−5.805	−2.917	2.888	7.675	−1006.124

2.6. FTIR spectrum

The most important FTIR spectral bands for azonaphthol dye **4** were recorded in the solid state employing the KBr disk method. The formation of azonaphthol dye **4** was demonstrated by its IR spectrum from the presence of a new band of azo stretching band (N=N) at 1500 cm^{-1}. The spectrum of the free amine (*p*-nitro aniline 1) exhibits a band at 3313 cm^{-1} which is assigned to a ν(N–H) group, the disappearance of this band due to being converted to an azo group by the coupling reaction. Furthermore, bands at the regions (1573–1624) cm^{-1} are attributed to ν(C=C) stretching band of aromatic rings. Figure 3 shows the FTIR spectrum of azonaphthol dye **4**.

2.7. Mass spectrum

Mass spectrum of azonaphthol dye **4** exhibits a signal with $m/z = 293$ which is very close to its calculated molecular weight $m/z = 294$ and the other fragments show a good consistent with the suggested structure. The other important peak at $m/z = 149$ probably due to loss of α-naphthol ($C_{10}H_{10}O$) from azonaphthol dye **4**. Therefore, the analysis of mass spectrum proved a good agreement with structure of the prepared azonaphthol dye **4**.

2.8. Quantum chemical calculations

The quantum chemical calculations for the synthesized azonaphthol dye **4** were obtained by using the Pentium (R)4/IPM-PC-CPU 3.00 GHz, 2.00 GB. The total energy of the molecules and their electronic properties such as the dipole moments, the energy of the highest occupied molecular orbital (EHOMO) and the lowest unoccupied molecular orbital (ELUMO) were determined via the Gaussian 09 software program with B3LYP/6-31G (d) within density functional theory (DFT) method [63]. The high value of EHOMO indicates that the molecule have great tendency to donate electrons. Whereas the low value of ELUMO shows the ability of accepting electrons to form stable bonds. The HOMO-LUMO energy calculations of synthesized azonaphthol dye **4** were carried out using DFT/B3LYP method with 6-31G(d) basis set, the shapes of orbital (HOMO- LUMO) and the energy gap between the HOMO-LUMO are a vital parameter to determine molecular electrical transport merits [64] that are plotted in 3D in figure 4 by using B3LYP/6-31 G(d) levels. The values of the calculated energies, dipole moment and the frontier molecular orbital energies of the compound from the B3LYP/6-31 G(d) basis set calculations are as given in table 1. Furthermore, the molecular electrostatic potential (MEP) and the electrostatic potential (ESP) maps of azonaphthol dye **4** were constructed for the most stable conformer at the same level of theory [DFT B3LYP/6-31 G(*d*)] (figure 5).

2.9. The UV–visible absorbance (A) spectrum

The azonaphthol dye **4** was dissolved in acetone with 10 mM concentration, and this sample concentration was used in all the measurements in present study. The UV–visible spectrum of the azonaphthol dye **4** solution at the

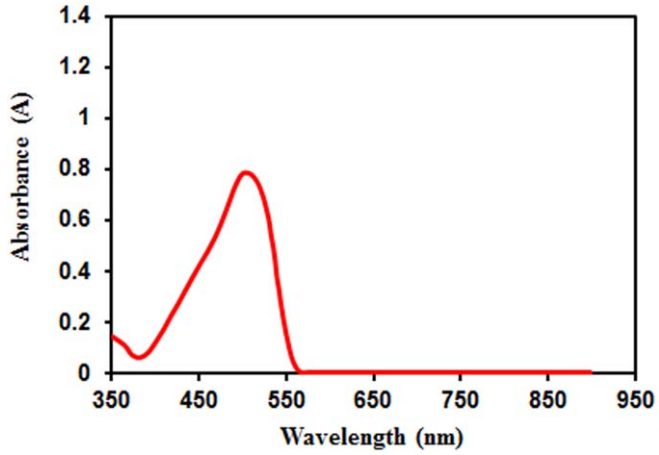

Figure 6. UV–visible absorbance spectrum of the azonaphthol dye **4** solution (at concentration of 10 mM).

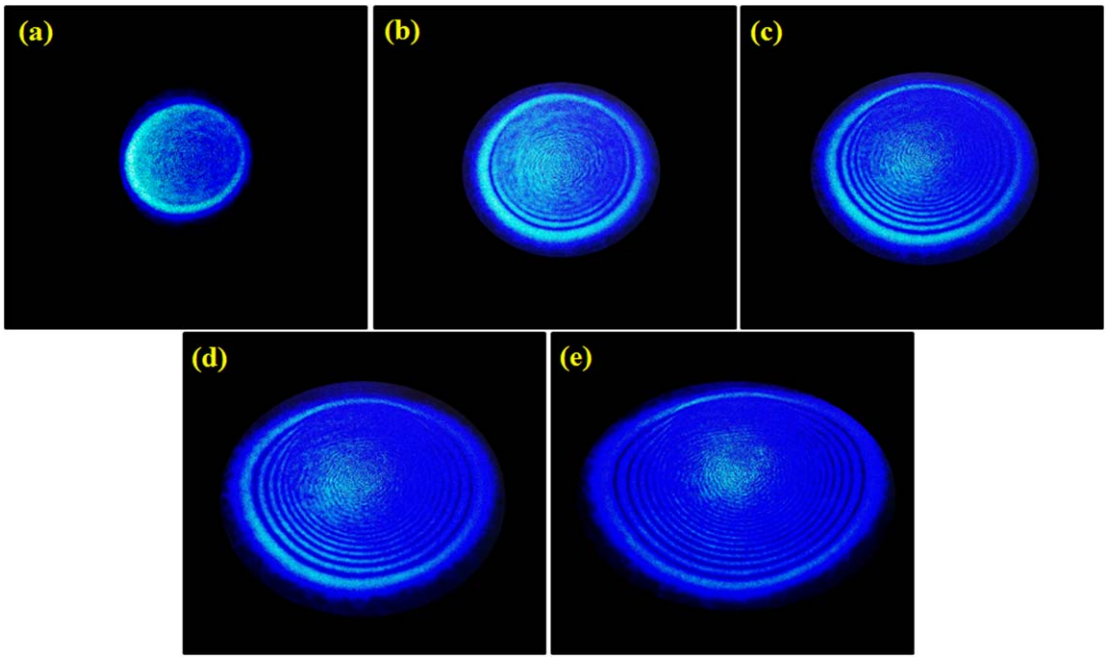

Figure 7. Diffraction ring patterns obtained in azonaphthol dye **4** solution (at concentration of 10 mM) against input power (mW) of (a) 7, (b) 15, (c) 25, (d) 29, (e) 42.

room temperature is shown in figure 6. It seems from this spectrum that the azonaphthol dye **4** solution has a maximum absorption at the wavelength range of 480–510 nm due to the π–π^* transition. The linear coefficient of absorption (α) of the compound at the wavelength 473 nm is calculated by using figure 6 and the equation [65]

$$\alpha = 2.303\frac{A}{d} \tag{1}$$

Where A and d are the azonaphthol dye **4** solution absorbance and thickness respectively. For $d = 1$ mm, $\alpha = 13.42\ \text{cm}^{-1}$.

3. Results

3.1. Diffraction ring patterns

Diffraction ring patterns obtained in the azonaphthol dye **4** solution for the input power (mW) of (a) 7, (b) 15, (c) 25, (d) 29, (e) 42 are displayed in figure 7. The dependence of interaction of laser beam with the azonaphthol dye **4** solution on it's wave front is depicted in figure 8, convergent and divergent when the sample was (a) 1 cm

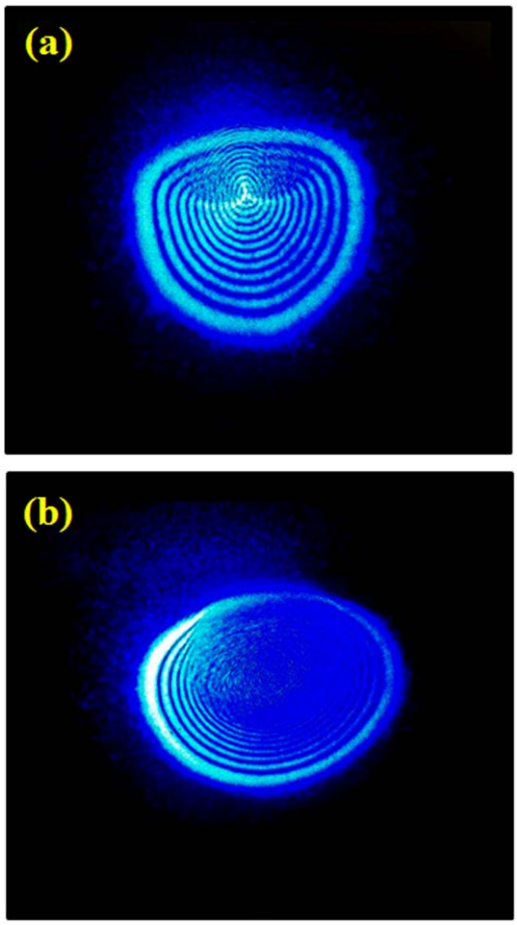

Figure 8. Diffraction ring patterns obtained when azonaphthol dye **4** solution (at concentration of 10 mM), cell was (a) 1 cm before and (b) 1 cm after the lens focus at input power of 42 mW.

before and (b) 1 cm after the lens focal point respectively, while the temporal evolution of the diffraction ring patterns are shown in figure 9. Inspection of figure 7 reveals that the ring patterns loses symmetry in the upper half as input power increases, such behavior is attributed to the increase of convection current in the vertical direction compared to the horizontal conduction one a results that have been observed recently [24]. The number of rings per each pattern increases as the input power increases where more heat resulted as absorption increases too so that the negative refractive index increase. As the input power of the laser beam increases so does the area of each pattern. It is noted that the outer most ring in each pattern is intense compare to the inner ones a manifestation of self-defocusing. From figure 8 it is proved that the type of interaction between the laser beam and the azonaphthol dye **4** solution is dependent on the type of the laser beam [66] or the field curvature viz., convergent when the sample situated before the focus of the lens and divergent when it is beyond the lens focal point. It is proved in figure 9, that each diffraction ring pattern evolves in time from small circular disc pattern to large circular one that breaks into circular diffraction ring pattern then to asymmetric pattern as time laps.

3.2. Z-scan

When conducting the OA Z-scan it is expected to obtain a saturation absorption if the measurements are made with a wavelength in which the sample possesses high absorption, that is near to the peak of absorption, or obtaining two photon absorption if the measurements are conducted at a wavelength in which the sample possesses a low absorption, that is far from the peak of absorption [67], and from figure 6 it is noted that our experiment was carried out at a wavelength near the peak of absorption, which is expected to obtain saturation absorption when carried out the OA Z-scan. Figure 10(a) represents the results of the azonaphthol dye **4** solution obtained from the OA Z-scan. As expected, saturation absorption obtained, as the figure 10(a) showed a maximum (peak) transmittance at $z = 0$, which indicates that it has a saturation absorption. But when performing the CA Z-scan it is expected to obtain a maximum transmittance followed by a minimum one if the material has a negative nonlinear index of refraction and a self-defocusing effect will occur to the laser beam, or obtain a minimum transmittance followed by a maximum one if the material has a positive nonlinear index of refraction and then create a self-focusing to the laser beam. Figure 10(b) shows the results obtained from the CA

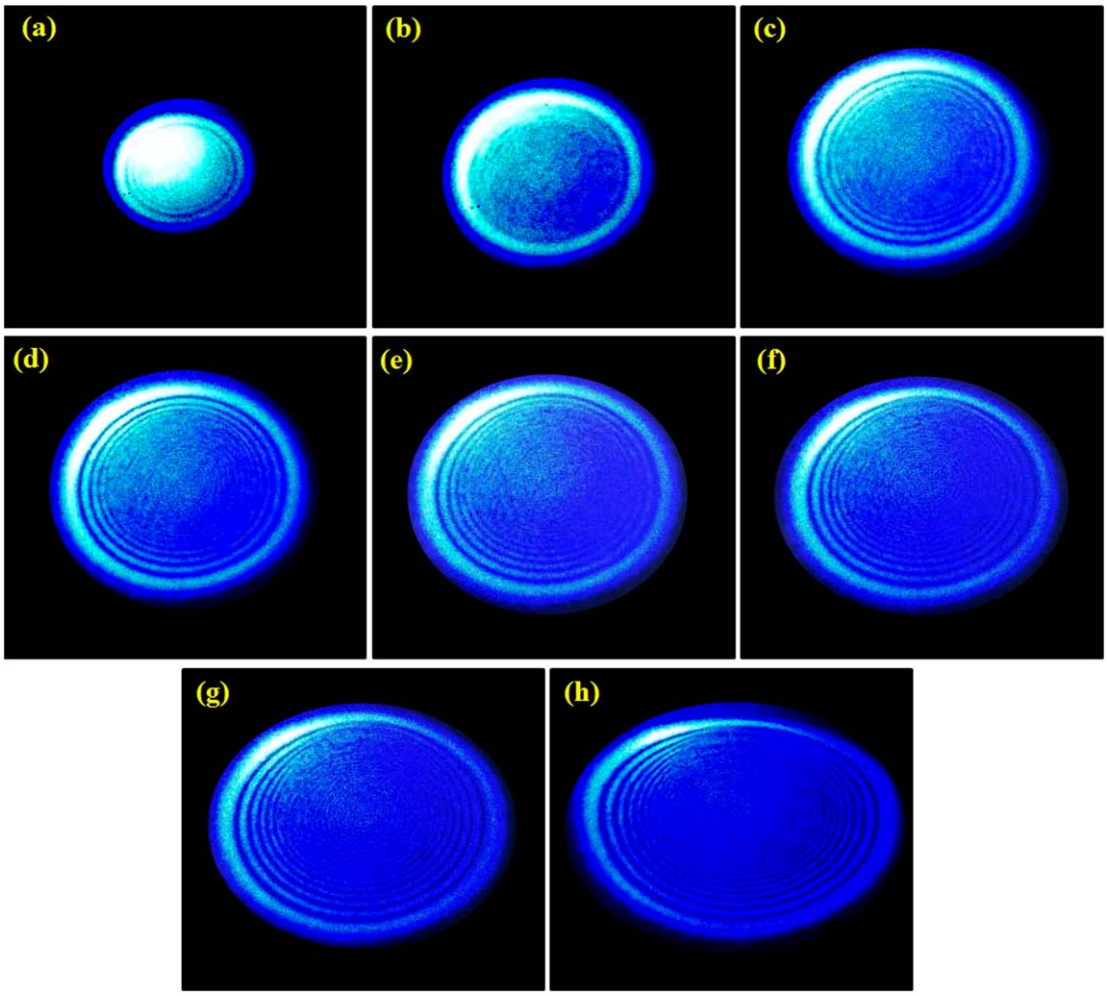

Figure 9. Temporal evolution of the ring pattern in azonaphthol dye **4** solution (at concentration of 10 mM) at input power of 42 mW (a) zero sec, (b) 100 msec, (c) 300 msec, (d) 500 msec, (e) 700 msec, (f) 800 msec, (g) 900 msec, (h) 1000 msec.

Z-scan where it shows a peak followed by a valley transmittances which ensures that the azonaphthol dye **4** solution has a negative nonlinear index of refraction and these results correspond to the results obtained in sub section 3.1. Figure 10(b) must be divided by figure 10(a) for the purpose of obtaining a pure nonlinear refractive index, since when conducting the CA Z-scan, the nonlinear coefficient of absorption and the nonlinear refractive index are affected. Figure 10(c) represents the result of dividing figure 10(b) by 10a.

3.3. Optical limiting

The human eye for people who work in a field that requires the use of laser and the optical sensors, will be exposed to damage due to the laser beam high intensity, so the human eye and optical sensor devices must be protected using an optical limiter, works to attenuate the laser beam that reaches both.

This device requires the manufacture of materials that have high transmittance at low incident power below the damage threshold, and low transmittance at high input power as they work to attenuate high input power. In this section the possibility of using the azonaphthol dye **4** solution as an optical limiter is tested by studying the optical limiting properties of the azonaphthol dye **4** solution. Figure 11(a) represents the relation between transmitted power through the azonaphthol dye **4** solution against input power. The sample possesses the properties of the optical limiter, as there are linear and nonlinear relations of the output power against the input power.

3.4. The nonlinear index of refraction, coefficient of nonlinear absorption and limiting threshold of the azonaphthol dye 4 solution

3.4.1. Diffraction ring patterns

To estimate the magnitude of the induced change in the sample refractive index, Δn, and the nonlinear index of refraction, n_2, from the experimental data it is assumed that the birth of any ring resulted indicate phase change

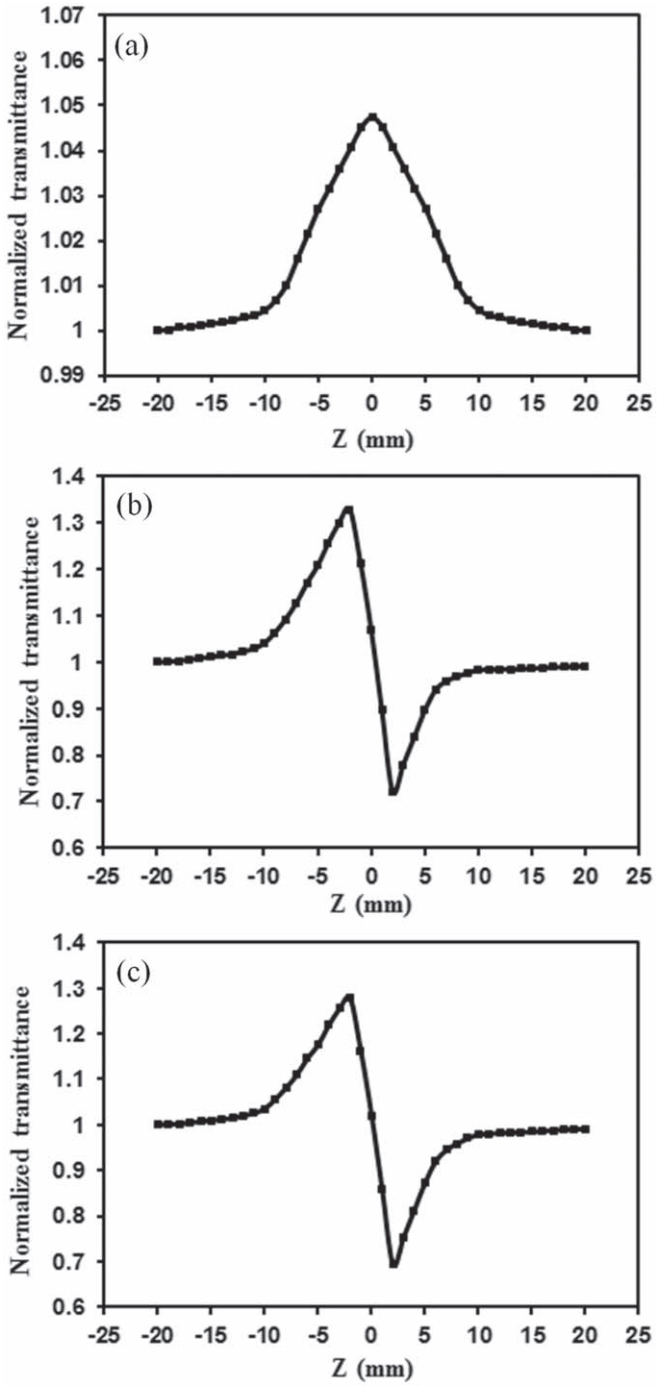

Figure 10. Experimental results for Z-scan of the azonaphthol dye **4** solution (at concentration of 10 mM) (a) OA Z-scan (b) CA Z-scan (c) division of (b) by (a).

of the laser beam by 2π radians as it traverses the nonlinear medium. For N rings the total on-axis change of the beam phase, $\Delta\varphi$, can be written as follows [68]:

$$\Delta\varphi = 2\pi N \tag{2}$$

$\Delta\varphi$ can be written in terms of Δn, the sample cell thickness, d, and the laser beam wave vector k ($=2\pi/\lambda$ and λ is the beam wavelength) as follows:

$$\Delta\varphi = k\Delta L \tag{3}$$

$$\Delta L = d\Delta n$$

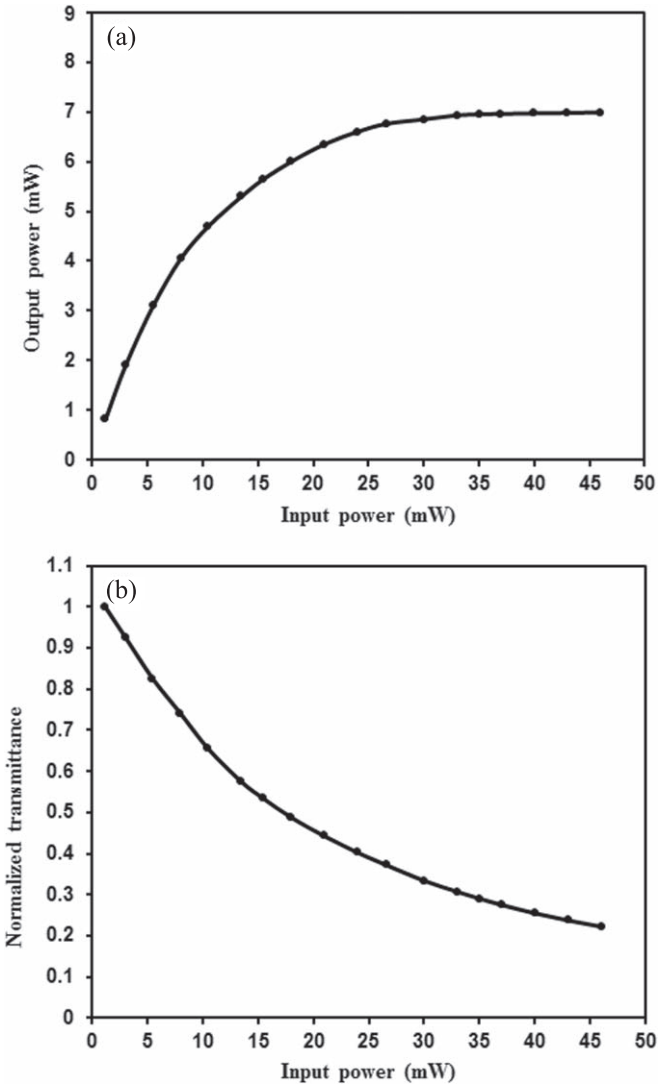

Figure 11. (a) Relation of the output power against the input power (b) The variation of the normalized transmittance against the input power of the azonaphthol dye **4** solution (at concentration of 10 mM).

So that

$$\Delta n = \frac{N\lambda}{d} \tag{4}$$

and

$$n_2 = \frac{\Delta n}{I} \tag{5}$$

I is the laser beam intensity ($=\frac{2P}{\pi\omega^2}$) and P is the input power.

For $N = 17$, input power, $P = 42$ mW, laser beam radius at the entrance of the sample cell, $\omega = 19.228$ μm, $I = 7235.7$ W cm^{-2}, $d = 0.1$ cm, $\lambda = 473$ nm, so that $\Delta n = 8.041 \times 10^{-3}$ and $n_2 = 1.11 \times 10^{-6}$ cm^2 W^{-1} for the azonaphthol dye **4** solution.

3.4.2. Z-scan

The nonlinear index of refraction, n_2, and the nonlinear coefficient of absorption, β, of the azonaphthol dye **4** solution in the case of the Z-scan method are respectively given by the following equations [23]

$$n_2 = \frac{\Delta\varphi\lambda}{2\pi L_{eff} I} \tag{6}$$

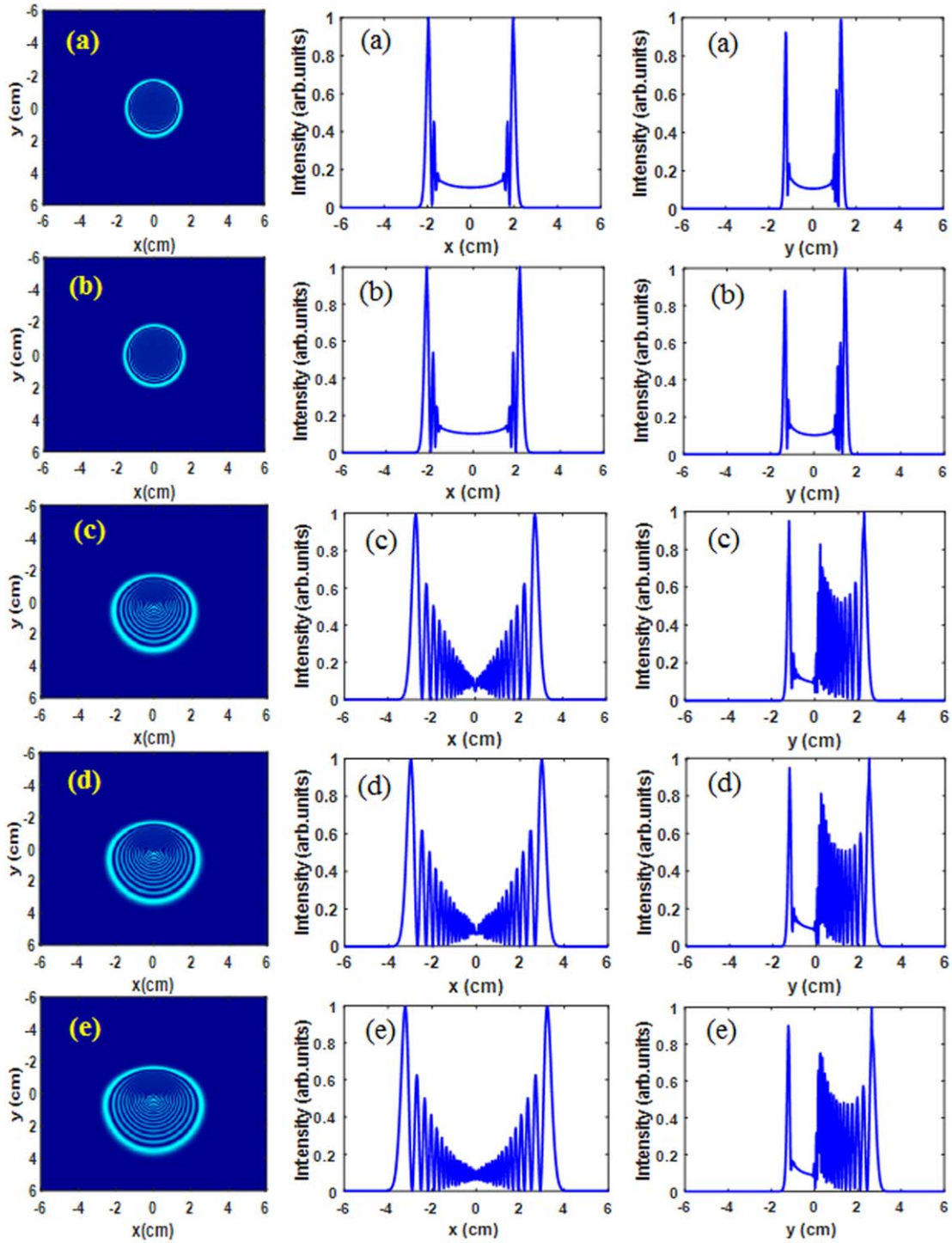

Figure 12. Calculated (left column) far-field intensity profile in azonaphthol dye **4** solution (at concentration of 10 mM) at input power (a) 7, (b) 15, (c) 25, (d) 29 and (e) 42 (mW), (middle column) one dimensional far-field intensity distribution in the x-direction and one (right column) dimensional far-field distribution of intensity in the y- direction respectively.

$$\beta = \frac{2\sqrt{2}\Delta T}{L_{eff} I} \tag{7}$$

where

$$\Delta T = 1 - T_p \tag{8}$$

$$\mathrm{L_{eff}} = [1 - \exp(-\alpha \mathrm{d})]/\alpha \tag{9}$$

$$|\Delta\varphi| = \frac{\Delta T_{p-\mathrm{v}}}{0.406(1 - S)^{0.25}} \tag{10}$$

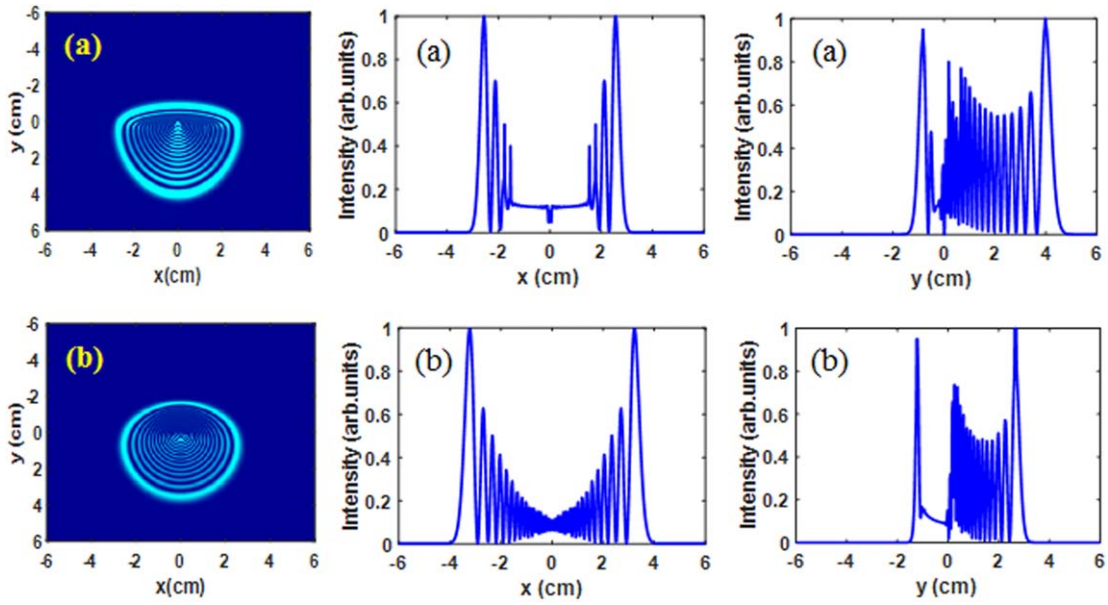

Figure 13. Calculated (left column) far-field intensity profile in azonaphthol dye **4** solution (at concentration of 10 mM) at input power of 42 mW, (middle column) one dimensional (x-axis) and (right column) one dimensional (y-axis) intensity distributions when the sample was (a) 1 cm before and (b) 1 cm after the lens focal point.

$$\Delta T_{p-v} = T_p - T_v \tag{11}$$

$$S = 1 - \exp\left(-\frac{2r_a^2}{\omega_a^2}\right) \tag{12}$$

where ΔT, L_{eff}, S, ΔT_{p-v}, r_a and ω_a, are one minus the peak transmittance (T_p) value in the OA Z-scan curve, the sample effective thickness, the aperture linear transmittance, the difference between the peak (T_p) and valley (T_v) transmittances in the CA Z-scan curve, the aperture radius and the beam radius at the aperture in the linear regime respectively. By using $P = 5$ mW, $I = 860.76$ W cm^{-2}, figures 10(a) and (c) and equations (6) to (12) the values of nonlinear index of refraction and the nonlinear coefficient of absorption of the azonaphthol dye **4** solution can be calculated and found equal 2.58×10^{-7} cm^2 W^{-1} and 2.83×10^{-3} cm W^{-1} respectively.

The discrepancy between n_2 values due to the ring patterns and Z-scan is attributed to the difference in input power used in both techniques where it was higher for diffraction ring pattern compare the Z-scan one. It is known that n_2 is intensity dependence so that $n_2 = 1.11 \times 10^{-6}$ cm^2 W^{-1} due to the former and $n_2 = 2.58 \times 10^{-7}$ cm^2 W^{-1} due to the later.

3.4.3. Calculations the optical limiting threshold

To calculate the threshold limiting, T_H, value of the azonaphthol dye 4 solution, which determines whether the azonaphthol dye **4** solution can be used as an optical limiter or not, and it is the value of the input power for which the transmittance is reduced to halve. Therefore, a curve must be drawn of the transmittance against the input power, from which the T_H can be found. Figure 11(b) depicts the transmittance against the input power. From the figure 11(b), the T_H of the azonaphthol dye **4** solution is equal to 17 mW.

3.5. Numerical calculation of the diffraction ring patterns

To simulate the experimentally obtained ring patterns due to the propagation of a visible laser beam with TEM_{00} mode, CW, low power, along the z-direction define the intensity profile, $I(r)$, of the form

$$I(r) = \frac{2P}{\pi\omega^2}\exp\left(-2\frac{r^2}{\omega^2}\right) \tag{13}$$

With P is input power peak, ω is the laser beam radius and $r = (x^2 + y^2)$ is the radial distance from the laser beam axis. At the entrance of the sample cell the laser beam complex field $E(x, y, t, z = 0)$ can be written as follows [69]

$$E(x, y, t, z = 0) = \left(\frac{2P}{\pi\omega^2}\right)^{1/2}\exp\left(-\frac{r^2}{\omega^2}\right)\exp\left(-ik\frac{r^2}{2R}\right) \tag{14}$$

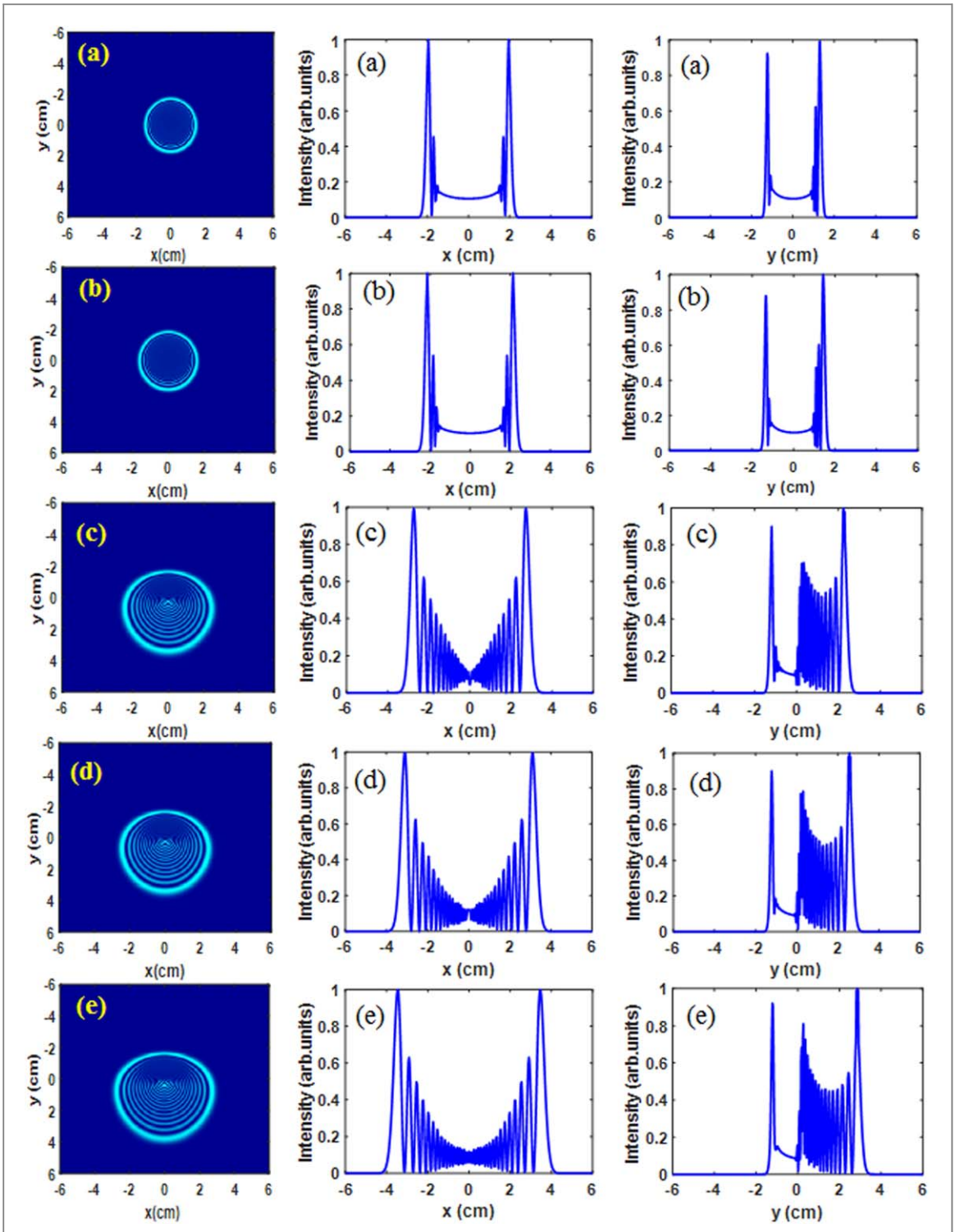

Figure 14. Calculated (left column) far-field intensity profile in azonaphthol dye **4** solution (at concentration of 10 mM), (middle column), one dimensional (x-axis) and (right column) one dimensional (y-axis) intensity distributions at input power of 42 mW (a) zero sec, (b) 100 msec, (c) 300 msec, (d) 500 msec, (e) 700 msec, (f) 800 msec, (g) 900 msec, (h) 1000 msec showing the temporal behavior.

R is the radius of laser beam wave front and $k = 2\pi/\lambda$ is the laser beam wave-vector. Due to the absorption coefficient, α, of the sample, part of energy the laser beam is absorbed and a heat is emitted in the sample locally in the shape of Gaussian extent. The heat is responsible for the increase of the liquid medium index of refraction, $n(x, y, t)$, depending on the thermo-optic coefficient, dn/dT, and the amount of temperature gradient, ΔT. The shift in the phase, $\Delta\varphi(x, y, t)$, of the laser beam as it passes through the medium might be written in terms of sample thickness, d, $n(x, y, t)$, and the initial linear refractive index of the medium, $n(0, 0, t)$ [59]. Taking these definitions into account, the laser beam complex field $E(x, y, t, z = 0)$ might be written as follows [59]:

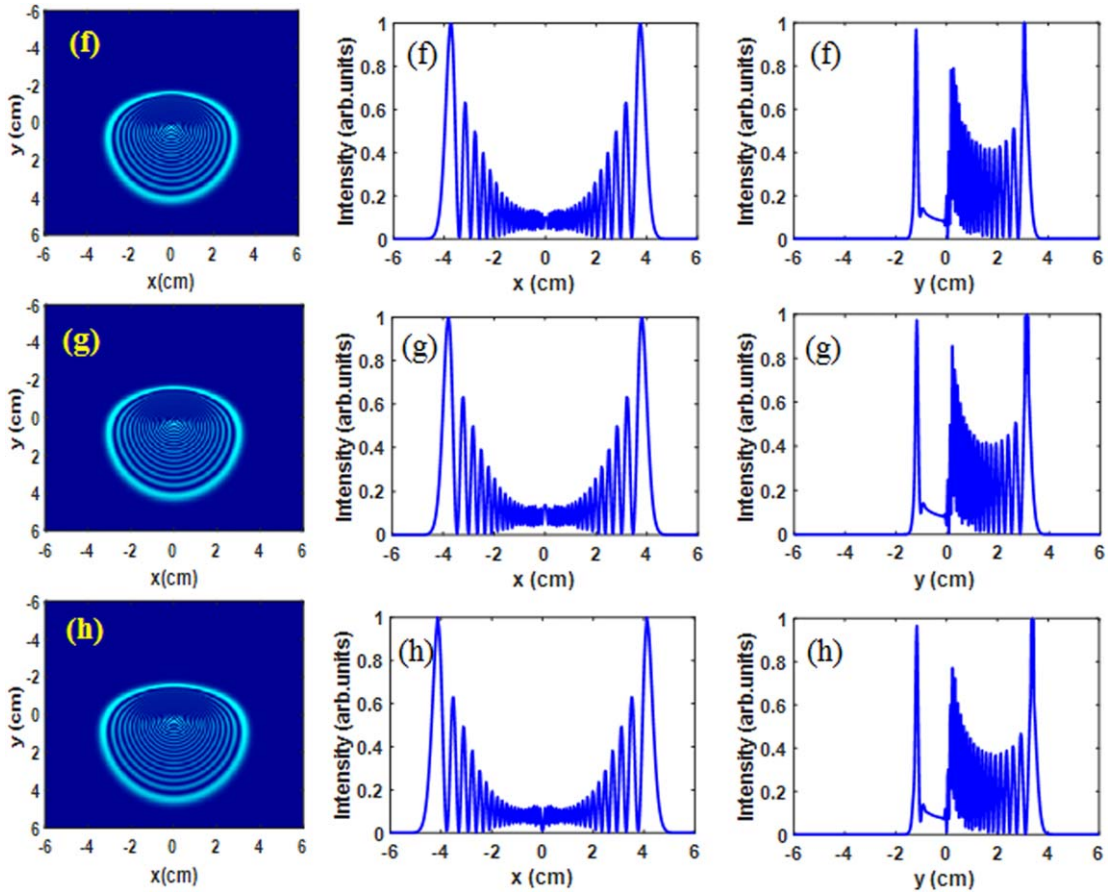

Figure 14. (Continued.)

$$E(x,\ y,\ t,\ z=0)=\left(\frac{2P}{\pi\omega^2}\right)^{\frac{1}{2}}\exp\left(-\frac{r^2}{\omega^2}\right)\exp\left(-ik\frac{r^2}{2R}\right)\exp(i\Delta\varphi(x,\ y,\ t)) \tag{15}$$

Since the screen was a distance D from the sample cell, the spatial coordinates $x,\ y$ are rewritten as $x',\ y'$ and via taking the effect of the convection current within the sample spatially and using the Fresnel- Kirchhoff theory, the laser beam intensity distribution on the screen, $I(x',\ y',\ t)$, can be written as follows [59]:

$$I(x',\ y',\ t)=\left|\left(\frac{2P}{\pi\omega^2}\right)^{\frac{1}{2}}\frac{i\pi\omega^2}{\lambda D}\exp(ikD)\exp\left(-\frac{\alpha d}{2}\right)\int_{-\infty}^{\infty}dx\int_{-\infty}^{\infty}dy\ .\ \exp\left(-\frac{x^2+y^2}{\omega^2}\right)\right.$$
$$\left.\ .\ \exp\left[i\left(-k\frac{x^2+y^2}{2R}\right)+\Delta\varphi(x,\ y,\ t)\right]\ .\ \exp\left(-ik\frac{xx'+yy'}{D}\right)\right|^2 \tag{16}$$

Equation (16) was solved numerically via the Mat Lab system. Figure 12 shows the numerically calculated diffraction ring patterns in the azonaphthol dye **4** solution at input power (mW) of (a) 7, (b) 15, (c) 25, (d) 29 and (e) 42. Figure 13 represent the calculated results of the effect of the beam wavefront (a) convergent, (b) divergent. Figure 14 shows the calculated results of the temporal evolution of a chosen ring pattern. The spatial variations of laser beam phase for the cases shown in figures 12–14 are shown in figures 15–17. When comparing figures 7–9 with figures 12–14 respectively overall agreements can be noticed between results of experiments and simulations respectively which are partly summarized in figure 18.

3.6. Mechanism for diffraction ring patterns, self-defocusing and optical limiting

The origin of the nonlinearity of the azonaphthol dye **4** solution is thermal in nature, because a CW laser beam was used in the current study, this thermally induced variation in refractive index causes spatial self-phase modulation (SSPM) in laser beam. Depending on the amount of phase shift that occurs to the laser beam, the SSPM causes diffraction ring patterns, self-focusing or self-defocusing. If the phase shift is $\geqslant 2\pi$, then the SSPM will produce diffraction ring patterns, and this explains the appearance of the diffraction ring patterns, but if the phase shift is less than 2π, then the SSPM lead to self-focusing or self-defocusing, and this explains the obtaining

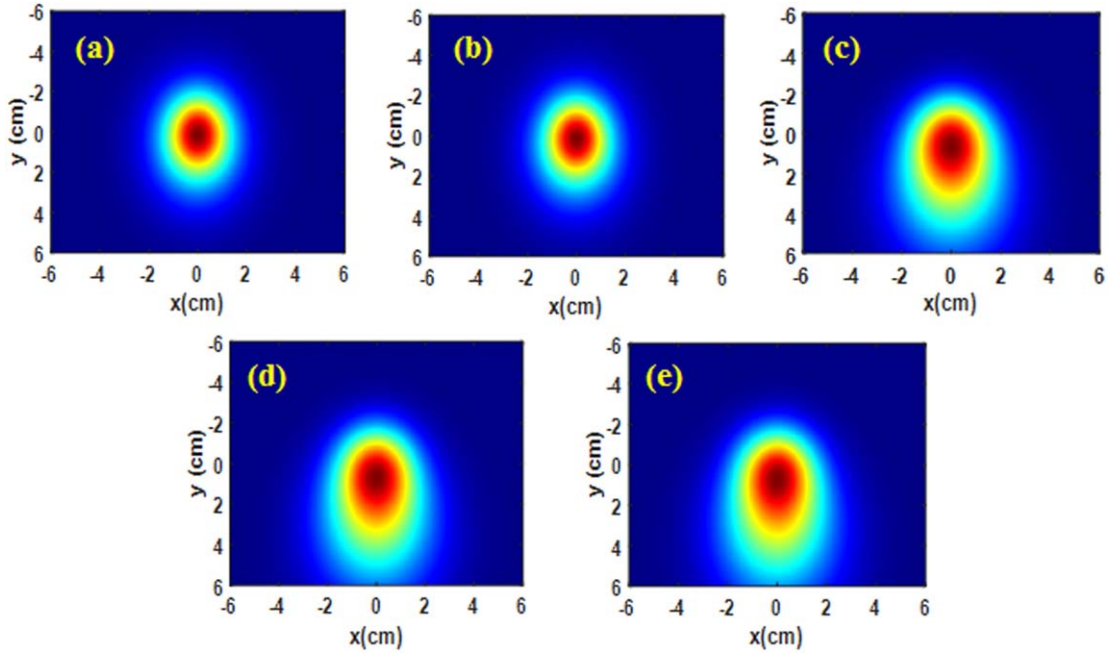

Figure 15. Calculated spatial phase distribution of the laser beam against input power (mW) (a) 7, (b) 15, (c) 25, (d) 29 and (e) 42 when the laser beam traverses the azonaphthol dye 4 solution (at concentration of 10 mM).

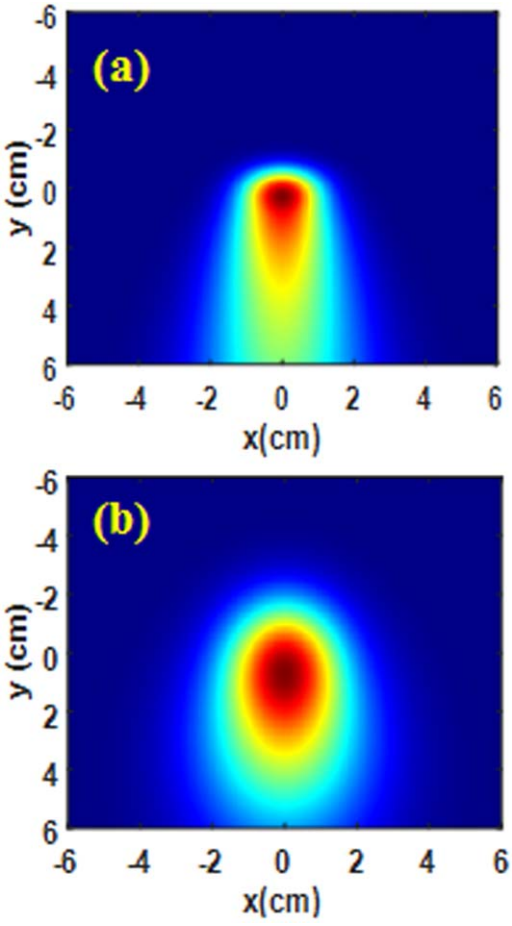

Figure 16. Calculated spatial phase distribution of input power of laser beam at 42 mW when the laser beam traverses the azonaphthol dye 4 solution (at concentration of 10 mM), where the sample was (a) 1 cm before and (b) 1 cm after the lens focal point.

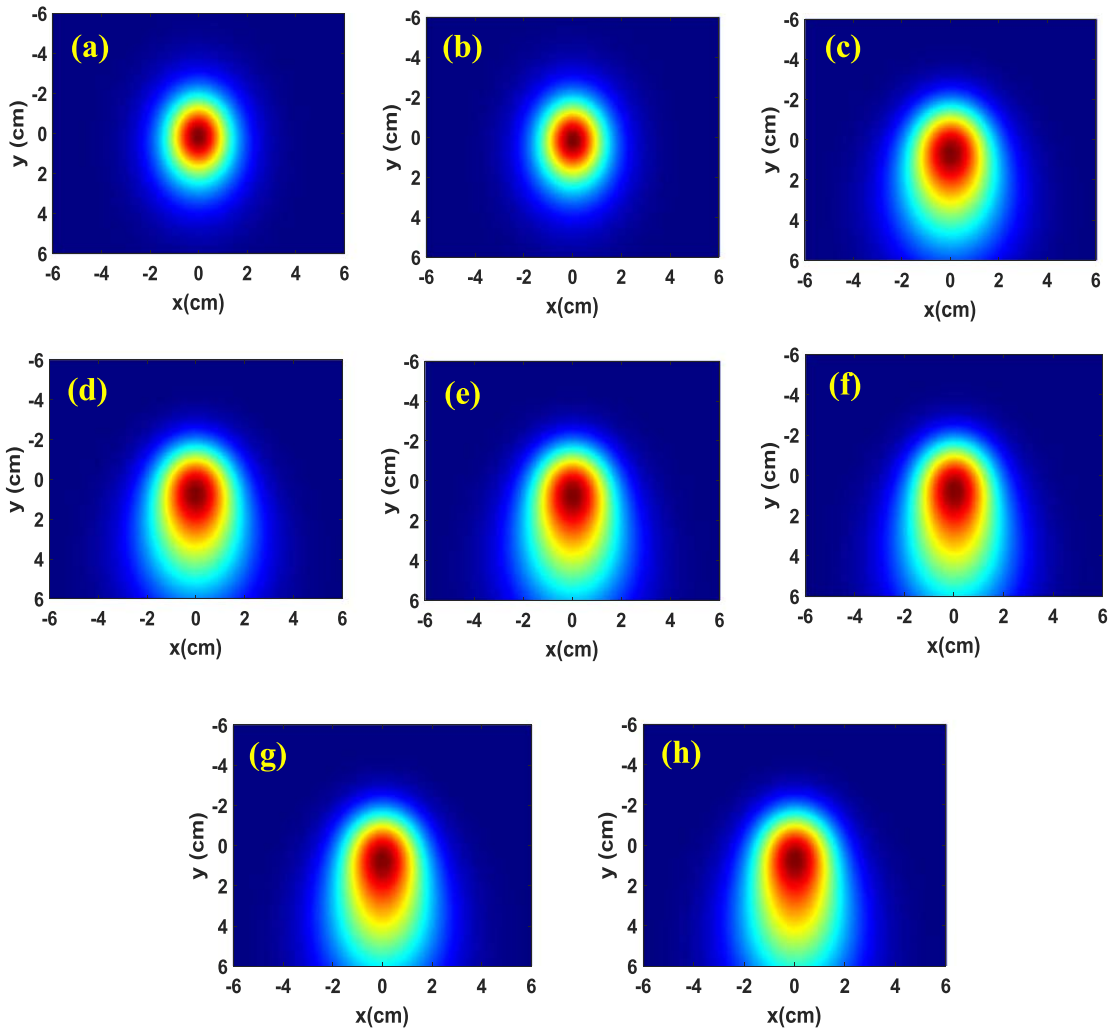

Figure 17. Calculated temporal spatial phase distribution of the laser beam at input of 42 mW (a) zero sec, (b) 100 msec, (c) 300 msec, (d) 500 msec, (e) 700 msec, (f) 800 msec, (g) 900 msec, (h) 1000 msec when the laser beam traverses the azonaphthol dye **4** solution (at concentration of 10 mM).

the self-defocusing in the Z-scan experiment. Due to this self-defocusing effect the transmittance recorded in the optical limiting experiment will be constant at high input power, so the nonlinear refraction is the mechanism responsible that the sample shows the optical limiter behavior.

4. Comparative study

The obtained values of the nonlinear index of refraction of the azonaphthol dye **4** solution which was measured using the Z-scan and the CW laser beam must be compared with other materials values known to have high values of the nonlinear index of refraction using the same method, because it is not possible to compare with materials used pulse laser, since the mechanism that lead to the appearance of nonlinearity is different, and this comparison is given in table 2. It is noted from table 2 that the value of the nonlinear index of refraction of the azonaphthol dye 4 solution is higher or of the same order compared to the materials mentioned in the table 2, which confirms that the advantage of the prepared azonaphthol dye **4** makes it a prime candidate for use in photonics.

5. Conclusion

The azonaphthol dye **4** was synthesized by coupling reaction from α-naphthol **3** (coupling partner) and benzenediazonium salt **2** (from *p*-nitro aniline 1) and this compound was confirmed using 1H NMR, FT-IR and Mass spectra techniques. The compound was also characterized by using a UV–visible absorption spectra. The passage of low power, CW, laser beam at wavelength 473 nm with fundamental mode through the azonaphthol

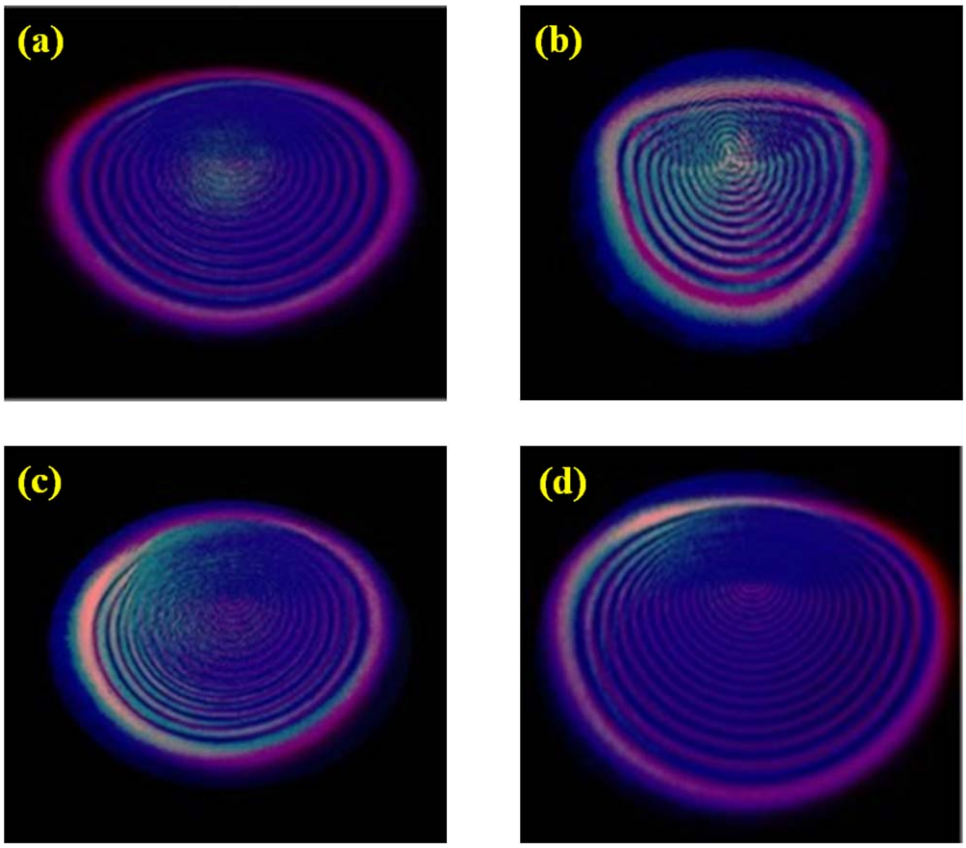

Figure 18. Direct comparison between experimental (blue) and calculated (red) chosen far-field intensity in azonaphthol dye 4 solution (at concentration of 10 mM) at (a) at input power 42 mW (b) when the sample was 1 cm before (c) the sample was 1 cm after the lens focal point and (d) steady state (1000 msec) or the field intensity at input power 42 mW.

Table 2. Comparison of the nonlinear refractive index value of the azonaphthol dye **4** solution with other materials based on the Z-scan technique.

Material	n_2 cm^2 W^{-1}	References
Azonaphthol dye 4 solution	2.58×10^{-7}	This work
$NiFe_2O_4$ nanoparticles	3.21×10^{-7}	[70]
Dihydropyridone solution	1.36×10^{-8}	[26]
Zinc sulfide nanoparticles	0.138×10^{-9}	[71]
PcCo(II)	7.79×10^{-9}	[24]
Cl-ANC doped PMMA	3.47×10^{-9}	[72]
Mo doped KTP	3.48×10^{-12}	[73]
GNS/ER composite	2.6×10^{-9}	[74]
PAn/PANr	6.5×10^{-9}	[75]
AG/PVA film	2.15×10^{-8}	[76]
$MoS_4Cu_4(Pz^{Me3})_6Cl_2$	4.09×10^{-9}	[77]
C_{60}/poly(ethylacetylenecarboxylate)	9.29×10^{-8}	[78]
Schiff base compound	6.44×10^{-8}	[79]
Chlorocurcumin solution	4.68×10^{-9}	[25]
ER/CB films	2.9×10^{-9}	[80]
Basic green 1 solution	1.63×10^{-7}	[81]
OpTpPzNi	1.13×10^{-8}	[82]
Nile blue chloride solution	9.15×10^{-7}	[83]
Chicago sky blue 6B doped PVA film	1.2×10^{-7}	[84]
Poly eosin-Y phthalate solution	2.83×10^{-7}	[85]

dye **4** solution have led to the generation of diffraction ring patterns. The number of rings in each pattern, area of each pattern and the loss of symmetry of each pattern are all proportional to the input power. Based on the number of rings and the Z-scan, the nonlinear refractive index of azonaphthol dye **4** solution was obtained

separately. Using the Fresnel-Kirchhoff theory and Fraunhofer approximations, simulation results of the diffraction ring patterns obtained with fine overall agreements. It is proved that the type of ring patterns are dependent on the laser beam wave front type. The azonaphthol dye **4** dissolved in acetone at concentration of 10 mM shows the property of optical limiter at the same wavelength.

ORCID iDs

Ahmed Majeed Jassem https://orcid.org/0000-0001-9892-2748
Qusay M A Hassan https://orcid.org/0000-0002-8941-6816

References

[1] Arivuoli D 2001 Fundamentals of nonlinear optical materials *Pramana* **57** 871–83
[2] Al-Mudhaffer M F, Al-Ahmad A Y, Hassan Q M A and Emshary C A 2016 Optical characterization and all-optical switching of benzenesulfonamide azo dye *Optik* **127** 1160–6
[3] Al-Asadi A S, Hassan Q M A, Abdulkader A F, Bakr H and Emshary C A 2020 Enhancement of the linear, nonlinear and optical limiting properties of epoxy resin decorated by zinc oxide nanoparticles *Phys. Scr.* **95** 085503 (12pp)
[4] Batagelj B, Janyani V and Tomazic S 2014 Research challenges in optical communications towards 2020 and beyond *J. Microelec. Elect. Comp. Mat.* **44** 177–84
[5] Zayets V 2017 High speed non-volatile optical memory achievements and challenges *Electronics* **6** 3–17
[6] Manickasundaram S, Kannan P, Kumaran R, Velu R, Ramamurthy P, Hassan Q M A, Palanisamy P K, Senthil S and Narayanan S S 2011 Holographic grating studies in pendant xanthene dyes containing poly(alkyloxymethacrylate)s *J. Mat. Sci: Mat. Electron.* **22** 25–34
[7] Manickasundaram S, Kannan P, Hassan Q M A and Palanisamy P K 2008 Azo dye based poly(alkyloxymethacrylate)s and their spacer effect on optical data storage *J. Mat. Sci: Mater Electron.* **19** 1045–53
[8] Manickasundaram S, Kannan P, Hassan Q M A and Palanisamy P K 2008 Holographic grating formation in poly(methacrylate) containing pendant xanthene dyes *Optoelec. Adv. Mat. Rap. Commun.* **2** 324–31
[9] Ali Q M, Palanisamy P K, Manickasundaram S and Kannan P 2006 Sudan IV dye based poly(alkyloxymethacrylate)films for optical data storage *Opt. Commun.* **267** 236–43
[10] Manshad R K H and Hassan Q M A 2012 Optical limiting properties of magenta doped PMMA under CW laser illumination *Adv. Appl. Sci. Res.* **3** 3696–702
[11] Hassan Q M A and Manshad R K H 2015 Optical limiting properties of sudan red B in solution and solid film *Opt. Quant. Electron.* **47** 297–311
[12] Hassan Q M A and Manshad R K H 2019 Surface morphology and optical limiting properties of azure B doped PMMA film *Opt. Mat.* **92** 22–9
[13] Hassan Q M A, Bakr H, Emshary C A and Sultan H A 2020 Studying the surface morphology, optical and nonlinear optical properties of epoxy resin doped nickel nitrate film *Optik* **213** 164771 (11 pp)
[14] Hassan Q M A 2017 Investigation on the nonlinear optical properties and optical power limiting of parsley oil *Int. J. Photo. Opt. Tech.* **3** 17–20
[15] Sultan H A, Hassan Q M A, Al-Asadi A S, Elias R S, Saeed H B B A and Emshary C A 2018 Far-field diffraction patterns and optical limiting properties of bisdemethoxycurcumin solution under CW laser illumination *Opt. Mater.* **85** 500–9
[16] Jebur J H, Hassan Q M A, Al-Mudhaffer M F, Al-Asadi A S, Elias R S, Saeed B A and Emshary C A 2020 The gamma radiation effect on the surface morphology and optical properties of alphamethyl curcumin: PMMA film *Phys. Scr.* **95** 045804 (10pp)
[17] Ali Q M and Palanisamy P K 2007 Optical phase conjugation by degenerate four-wave mixing in basic green 1 dye-doped gelatin film using He–Ne laser *Opt. Las. Technol.* **39** 1262–8
[18] Ali S A, Hassan Q M A, Emshary C A and Sultan H A 2020 Characterizing optical and morphological properties of eriochrome black T doped polyvinyl alcohol film *Phys. Scr.* **95** 095814 (11pp)
[19] Hassan Q M A 2007 Third-order nonlinearities and optical limiting properties of rose bengal at 532 nm wavelength *J. Bas. Res. (Sci.)* **33** 76–82
[20] Saeed B A, Hassan Q M A, Emshary C A, Sultan H A and Elias R S 2020 The nonlinear optical properties of two dihydropyridones derived from curcumin *Spectrochim. Acta, Part A: Mol. Biomol. Spectrosc.* **240** 118622 (14 pp)
[21] Hassan Q M A 2014 Two-photon absorption-based optical limiting in 2-(2-methoxybenzyllideneamino)-5-methylphenylmercuric chloride-doped PMMA film *Mod. Phys. Lett.* B **28** 1450079 (10 pp)
[22] Callen W R, Huth B G and Pantell R H 1967 Optical patterns of thermally self-defocused light *Appl. Phys. Lett.* **11** 103–5
[23] Sheik-Bahae M, Said A A, Wei T, Hagan D J and Van E W 1990 Stryland, Sensitive measurement of optical nonlinearities using a single beam *IEEE J. Quant. Electron.* **26** 760–9
[24] Kadhum A J, Hussein N A, Hassan Q M A, Sultan H A, Al-Asadi A S and Emshary C A 2018 Investigating the nonlinear behavior of cobalt (II) phthalocyanine using visible CW laser beam *Optik* **157** 540–50
[25] Elias R S, Hassan Q M A, Sultan H A, Al-Asadi A S, Saeed B A and Emshary C A 2018 Thermal nonlinearities for three curcuminoids measured by diffraction ring patterns and Z-scan under visible CW laser illumination *Opt. Las. Techn.* **107** 131–41
[26] Elias R S, Hassan Q M A, Emshary C A, Sultan H A and Saeed B A 2019 Formation and temporal evolution of diffraction ring patterns in a newly prepared dihydropyridone *Spectrochim. Acta, Part A: Mol. Biomol. Spectrosc.* **223** 117297 (16 pages)
[27] Sultan H A, Hassan Q M A, Bakr H, Al-Asadi A S, Hashim D H and Emshary C A 2018 Thermal-induced nonlinearities in rose, linseed and chamomile oils using CW visible laser beam *Can. J. Phys.* **96** 157–64
[28] Al-Timimy K A, Hassan Q M A, Sultan H A and Emshary C A 2020 Solvents effect on the optical nonlinear properties of the sudan iv *Optik* **224** 165398 (15 pp)
[29] Shridhar A H, Keshavayya J, Hoskeri H J and Shoukat Ali R A 2011 Synthesis of some novel bis 1, 3, 4-oxadiazole fused azo dye derivatives as potent antimicrobial agents *Int. Res. J. Pure. Appl. Chem.* **1** 119–29
[30] Matada M N and Jathi K 2019 Pyrazole-based azo-metal(II) complexes as potential bioactive agents: synthesis, characterization, antimicrobial, anti-tuberculosis, and DNA interaction studies *J. Coord. Chem.* **72** 1994–2014

[31] Avci G A, Ozkinali S, Ozluk A, Avci E and Kocaokutgen H 2012 Antimicrobial activities, absorption characteristics and tautomeric structures of o, o'-hydroxyl azo dyes containing an acryloyloxygroup and their chromium complexes *Hacettepe J. Biol. Chem.* **40** 119–26

[32] Cankar P, Popa I, Travnicek Z, Styskala J, Hradil P and Slouka J 2013 Synthesis of 1-aminocodeine as a synthon for other codeine derivatives *Eur. J. Org. Chem.* **27** 6062–8

[33] Mooter G, Maris B, Samyn C, Augustijns P and Kinget R 1997 Use of Azo polymers for colon-specific drug delivery *J. Pharm. Sci.* **86** 1321–7

[34] Burland D M, Miller R D and Walsh C A 1994 Second-order nonlinearity in poled-polymer systems *Chem. Rev.* **94** 31–75

[35] Ikeda T and Tsutsumi O 1995 Optical switching and image storage by means of azobenzene liquid-crystal films *Science* **268** 1873–5

[36] Kim D Y, Tripathy S K, Li L and Kumar J 1995 Laser-induced holographic surface relief gratings on nonlinear optical polymer films *Appl. Phys. Lett.* **66** 1166–8

[37] Chigrinov V, Kwok H S, Takada H and Takatsu H 2005 Photo-aligning by azo-dyes: physics and applications *Liquid Crystals Today* **14** 1–15

[38] Tomás-Gamasa M, Martínez-Calvo M, Couceiro J R and Mascareñas J L 2016 Transition metal catalysis in the mitochondria of living cells *Nat. Commun.* **7** 1–14

[39] García-Iriepa C, Marazzi M, Frutos L M and Sampedro D 2013 E/Z photochemical switches: syntheses, properties and applications *RSC Adv.* **3** 6241–66

[40] Al-Juaid S S and Azo M 2007 Dyes compounds as corrosion inhibitors for dissolution of aluminium in sodium hydroxide solutions *Port. Electro. Acta.* **25** 363–73

[41] Jassim A M and Jaber M Q M H A 2012 Synthesis and characterization of Novel Schiff bases and evaluation of corrosion inhibitors and biological activity *J. Thi-Qar Sci.* **3** 64–75

[42] Peme T, Olasunkanmi L O, Bahadur I, Adekunle A S, Kabanda M M and Ebenso E E 2015 Adsorption and corrosion inhibition studies of some selected dyes as corrosion inhibitors for mild steel in acidic medium: gravimetric, electrochemical, quantum chemical studies and synergistic effect with iodide ions *Molecules* **20** 16004–29

[43] Kooh M R R, Yoong V N and Ekanayake P 2014 Density functional theory (DFT) and time-dependent density functional theory (TDDFT) studies of selected ancient colourants as sensitizers in dye-sensitized solar cells *J. Natl. Sci. Found. Sri.* **42** 169–75

[44] Brzozowski L and Sargent E H 2001 Azobenzenes for photonic network applications: third-order nonlinear optical properties *J. Mat. Sci.: Mat. Electron.* **12** 483–9

[45] Motaghni F and Abed Y 2018 Synthesis and investigation of nonlinear optical properties of para red: Z-scan technique and quantum mechanical calculations *Mat. Sci. Poland* **36** 445–51

[46] Morales-Saavedra O G, Garcia T, Caicedo C and Rivera E 2010 Nonlinear optical properties of novel amphiphilic azo-polymers bearing well defined oligo (ethylene glycor) spacers *Rev. Maxi. Fisi.* **56** 449–55

[47] Nataj N H, Mokajerani E, Nemati H, Moheghi A, Yazdanbakhsh M R, Goli M and Mohammadi A 2013 Studying optical and and nonlinear optical properties of synthesized azo dyes doped in polymer and Z-scan techniques *Appl. Poly. Sci.* **127** 456–62

[48] Esme A and Sagdinc S 2014 The linear and nonlinear optical properties and quantum chemical parameters of some sudan dyes *BAÜ Fen Bil. Enst. Dergisi Cilt.* **16** 47–75

[49] Li H, Bi Z-T, Fu W-Y, Xu R-F, Zhang Y, Shen X, Li M-X, Tang G and Han K 2017 Theoretical study of the spectroscopic optical properties of trans-and cis-4-hydroxya-zobenzene *J. Mol. Model.* **23** 79 (8pp)

[50] Heydari E, Mohajerani E and Shams A 2011 All optical switching in azo-polymer planar waveguide *Opt. Commun.* **264** 1208–12

[51] Aithal S, Aithal P S and Bhat G K 2016 A review on organic materials for optical phase conjugation and all-optical switches *Int. J. Manag. IT Eng.* **6** 222–38

[52] Merino E 2011 Synthesis of azobenzenes: the coloured pieces of molecular materials *Chem. Soc. Rev.* **40** 3835–53

[53] Nicoletta F P, Cupelli D, Formoso P, De Filpo G, Colella V and Guzliuzza A 2012 Light responsive polymer membranes: a review *Membranes* **2** 134–97

[54] Julkapli N M, Bagher S and Bee Abd Havnid S 2014 Recent advances in heterogeneous photocatalytic decolorization of synthetic dyes *The Sci. Wo. J.* **2014** 692307 (25pp)

[55] Fleischmann C, Lievenbruck M and Ritter H 2015 Polymers and dyes: development and applications *Polymers* **7** 717–46

[56] Chomicki D, Kharchenko O, Showronski L, Kowalonek J, Kozanecka- Szmigiel A, Szmigiel D, Smokal V, Krupka O and Derkowska-Zielinska B 2020 Physico-chemical and light induced properties of quinolone azo-dyes polymera *Int. J. Molec. Sci.* **21** 57 (19pp)

[57] Valligatla S, Haldar K K, Patra A and Desai N R 2016 Nonlinear optical switching and optical limiting in colloidal CdSe quantum dots investigated by nanosecond Z-scan measurement *Opt. Las. Tech.* **84** 87–93

[58] Al-Deen I, Al-Saidi H and Abdulkareem S A 2015 Nonlinear optical properties and optical power limiting behavior of Leishman dye in solution and solid polymer film using zscan *Optik* **126** 4299–303

[59] Motiei H, Jafari A and Naderali R 2017 Third-order nonlinear optical properties of organic azo dyes by using strength of nonlinearity parameter and Z-scan technique *Optics & Las. Tech.* **88** 68–74

[60] Aziz M S and Mallah H M E 2009 Electrical and optical properties of azo dye *Ind. J. Pure Appl. Phys.* **47** 530–4

[61] Rosalyn P D S, Senthil S, Kannan P, Vinitha G and Ramalingam A 2007 Investigation on substituent effect in novel azo-naphthol dyes containing polymethacrylates for nonlinear optical studies *J. Phys. Chem. Sol.* **68** 1812–20

[62] Esme A and Sagdinc S G 2014 The linear, nonlinear optical properties and quantum chemical parameters of some sudan dyes *Bau Fen Bil Enst Dergisi Cilt* **16** 47–75

[63] Jassem A M, Radhi W A, Jaber H A and Mohammed F J 2013 Synthesis and characterization of 1,3,4-oxadiazoles derivatives from 4-phenyl-semicarbazide *J. Bas. Res. (Sciences)* **39** 158–70

[64] Jassem A M, Raheemah A H, Radhi W A, Ali A M and Jaber H A 2019 Highly diastereoselective metal-free catalytic synthesis of drug-like spiroimidazolidinone *Rus. J. Org. Chem.* **55** 1598–603

[65] Abu A, El-Fadl, Mohamad G A, Abd El-Moiz A B and Rashad M 2005 Optical constants of $Zn_{1-x}Li_xO$ films prepared by chemical bath deposition technique *Physica* B **366** 44–54

[66] Santamato E and Shen Y R 1984 Field-curvature effect on the diffraction ring pattern of a laser beam dressed by spatial self-phase modulation in a nematicfilm *Opt. Lett.* **9** 564–6

[67] Umakanta Tripathy S and Bisht P B 2006 Simultaneous estimation of optical nonlinear refractive and absorptive parameters by solvent induced changes in optical density *Opt. Commun.* **261** 353–8

[68] Ogusu K, Kohtani Y and Shao H 1996 Laser-induced diffraction rings from an absorbing solution *Opt. Rev.* **3** 232–4

[69] Karimzadeh R 2012 Spatial self-phase modulation of a laser beam propagation through liquids with self-induced natural convection flow *J. Opt.* **14** 095701 (9 pp)
[70] Dehghani Z, Parishani M, Nadafan M, Anvari J Z and Malekfa R 2017 Third-order nonlinear optical properties of $NiFe_2O_4$ nanoparticles by Z-scan technique *Optik* **144** 672–8
[71] Dehghani Z, Nazerdeylami S, Saievar-Iranizad E and Majles Ara M H 2011 Synthesis and investigation of nonlinear optical properties of semiconductor ZnS nanoparticles *J. Phys. Chem. Sol.* **72** 1008–10
[72] Maidur S R and Shankaragouda Patil P 2019 Linear optical and third-order nonlinear optical properties of anthracene chalcone derivatives doped PMMA thin films *Optik* **190** 54–67
[73] Rajeev Gandhi J, Rathnakumari M, Ramamurthi K, Ramesh Babu R, Sastikumar D and Sureshkumar P 2014 Measurement of nonlinear refractive index of pure and doped KTP crystals by Z-scan technique using cw He–Ne laser *Optik* **125** 6462–5
[74] Al-Asadi A S, Hassan Q M A, Abdulkader A F, Mohammed M H, Bakr H and Emshary C A 2019 Formation of graphene nanosheets/epoxy resin composite and study its structural, morphological and nonlinear optical properties *Opt. Mat.* **89** 460–7
[75] Hussain M S, Hassan Q M A, Sultan H A, Al-Asadi A S, Chayed H T and Emshary C A 2019 Preparation, characterization, and study of the nonlinear optical properties of a new prepared nanoparticles copolymer *Mod. Phys. Let.* B **33** 1950456 (17 pp)
[76] Hassan Q M A 2018 Study of nonlinear optical properties and optical limiting of acid green 5 in solution and solid film *Opt. Las. Tech.* **106** 366–71
[77] Sadr M H, Mohammadi V M, Soltani B, Jamshidi-Ghaleh K and Mousavi S Z 2016 Nonlinear optical responses of $MoS_4Cu_4(Pz^{Me3})_6Cl_2$ under lowpower CW He-Ne laser excitation *Optik* **127** 6050–5
[78] Zidan M D, Alsous M B, Allaf A W, Allahham A, AL-Zier A and Rihawi H 2016 Z-scan measurements of the third order optical nonlinearity of C60doped poly(ethylacetylenecarboxylate) under CW regime *Optik* **127** 2566–9
[79] Almashal F A, Mohammed M Q, Ali Hassan Q M, Emshary C A, Sultan H A and Dhumad A M 2020 Spectroscopic and thermal nonlinearity study of a Schiff base compound *Opt. Mat.* **100** 109703 (12pp)
[80] Abdulkader A F, Hassan Q M A, Al-Asadi A S, Bakr H, Sultan H A and Emshary C A 2018 Linear, nonlinear and optical limiting properties of carbon black in epoxy resin *Optik* **160** 100–8
[81] Ali Q M and Palanisamy P K 2005 Investigation of nonlinear optical properties of organic dye by Z-scan technique using He–Ne laser *Optik* **116** 515–20
[82] Hassan Q M A, Sultan H A, Al-Asadi A S, Kadhim A J, Hussein N A and Emshary C A 2019 Synthesis, characterization, and study of the nonlinear optical properties of two new organic compounds *Synth. Met.* **257** 116158 (14 pp)
[83] Ali Q M and Palanisamy P K 2006 Z-scan determination of the third-order optical nonlinearity of organic dye nile blue chloride *Mod. Phys. Lett.* B **20** 623–32
[84] Hassan Q M A 2008 Nonlinear optical and optical limiting properties of chicago sky blue 6B doped PVA film at 633 nm and 532 nm studied using a continuous wave laser *Mod. Phys. Lett.* B **22** 1589–97
[85] Shabeeb G M, Emshary C A, Hassan Q M A and Sultan H A 2020 Investigating the nonlinear optical properties of poly eosin-Y phthalate solution under irradiation with low power visible CW laser light *Physica* B **578** 411847 (13pp)